Cenozoic uplift of the Hoggar Region, North Africa: constraints from its northern flank (Illizi basin, Algeria)

Kara L. English

Petroceltic International Plc, 5th Floor, 3 Grand Canal Plaza, Grand Canal Street Upper, Dublin 4, Ireland. Phone: +353 1 421 8300; E-mail: kara.english@yahoo.ca

Jonathan Redfern

School of Earth, Atmospheric and Environmental Sciences, University of Manchester, Williamson Building, Oxford Road, Manchester, M13 9PL, United Kingdom; E-mail: jonathan.redfern@manchester.ac.uk

Giovanni Bertotti

Geoscience and Engineering, Delft University of Technology, Stevinweg 1, 2628CN, Delft, The Netherlands; E-mail: G.Bertotti@tudelft.nl

Joseph M. English

Petroceltic International Plc, 5th Floor, 3 Grand Canal Plaza, Grand Canal Street Upper, Dublin 4, Ireland. Phone: +353 1 421 8300; E-mail: joseph.english@petroceltic.com

Rachida Yahia Cherif

Direction Coordination Groupe Associations – Sonatrach, Djenane El-Malik, Hydra, Alger, Algérie (Algeria); E-mail: Rachida.Yahiacherif@Sonatrach.dz

Submitted to *Basin Research*, July 27th, 2015

Revision submitted to *Basin Research*, November 13, 2015

Second Revision submitted to *Basin Research*, January 3, 2016

Main text word count = 5960

Abstract word count = 182

Number of references = 85

Number of tables = 3

Number of figures = 7

Data Repository = Yes

Corresponding author = Kara English

ABSTRACT

Zones of anomalously high topography within continental interiors, distant from active plate boundaries, are interpreted as being either dynamically supported by viscous flow in the underlying mantle or influenced by plate tectonics. Constraining the models of their genesis requires accurate data on the timing and dimensions of such features. New apatite fission-track and thermal maturity data from the Illizi Basin in Algeria quantifies the magnitude and timing of kilometre-scale uplift and exhumation of the northern flank of the Hoggar swell in North Africa. The findings of this study, integrated with previously published thermochronological data, confirm that long wavelength regional uplift occurred during the Cenozoic extending over a distance in excess of 1,500 km from north to south. The uplift evidenced in the Hoggar Massif significantly impacted the flanking Illizi and Tim Mersoï basins. The combination of thermal history modelling and regional stratigraphic observations indicates that the onset of exhumation of the Illizi Basin likely occurred during the Eocene, broadly coincident with magmatism on the Hoggar Massif to the south and the onset of tectonic shortening in the Atlasic belt to the north.

INTRODUCTION

Zones of anomalously high topography within continental interiors, far away from active plate boundaries, are often interpreted as being dynamically supported by viscous flow in the underlying mantle (e.g. Braun, 2010; Al-Hajri *et al.*, 2009; Moucha & Forte, 2011; Jones *et al.*, 2012). The average diameter of modern topographic swells across Africa and Antarctica is 1850 ± 450 km, and associated gravity anomalies suggest that the full height of dynamically supported topography ranges from 800 to 1800 m (Jones *et al.*, 2012). Long-wavelength basins and swells characterize the present-day topography of Africa (Holmes, 1944; Burke, 1996). Northern Africa is characterised by a number of prominent topographic swells, typically associated with relatively young (c. 35 Ma-Recent) volcanism (e.g. Hoggar, Tibesti, Darfur; Fig. 1), consistent with the involvement of sublithospheric processes (Sahagian, 1988; Wilson & Guiraud, 1992; Burke, 1996; Liégeois *et al.*, 2005; Azzouni-Sekkal *et al.*, 2007; Beccaluva *et al.*, 2007).

There is general consensus that mantle convection plays an important role in the formation of many modern topographic swells, but detailed surface studies are required to establish the timing and evolution of these uplifts in the geological record to provide constraints for understanding their genesis. The Hoggar Massif in central North Africa (Fig. 1) is characterized by exposed crystalline basement, and flanked by sedimentary basins. New apatite fission-track and thermal maturity data from a well in the Illizi Basin (Well A; Fig. 1), along with basin modelling and regional stratigraphic correlations, constrain both the timing and magnitude of exhumation of the northern flank of the Hoggar Massif. These new data are integrated with previously published thermochronological data from the Hoggar Massif and surrounding basins. A regional cross-section is constructed from the Illizi and Berkine basins in the north, over the Hoggar Massif, and southward across the Tim Mersoï and Iullemmeden basins (Fig. 1). This illustrates that the Cenozoic kilometric-scale rock uplift occurred over a distance in excess of 1,500 km from north to south.

GEOLOGICAL SETTING

The Hoggar Massif in Algeria is associated with exposed Pan-African basement extending over an area greater than 400,000 km^2 (Fig. 1). The preserved Paleozoic sections north and south

of the Hoggar Massif have broadly similar stratigraphy, with up to 2.5 km of sedimentary section preserved in the Illizi Basin (Galeazzi *et al.*, 2010) to the north and in the Iullemmeden and Tim Mersoï basins (Zanguina *et al.*, 1998) to the south. A predominance of northerly paleocurrent directions reported within Cambro-Ordovician and Devonian sandstones on the northern and southern sides of the Hoggar Massif (Beuf *et al.*, 1971) suggests that the Hoggar Massif was not a structural high during the earlier part of the Paleozoic, and that sequences were originally deposited continuously across the Hoggar region. Following the collision of Gondwana with Laurasia, the Paleozoic sequence was variably uplifted and eroded across parts of northwest Africa during the Late Carboniferous-Early Permian Hercynian (Variscan) Orogeny (Aliev *et al.*, 1971; Burollet *et al.*, 1978; Boote *et al.*, 1998; Acheche *et al.*, 2001).

Rifting along the northern margin of the African plate during the Early Triassic records the initial breakup of Gondwana and the opening of the Tethyan seaway (e.g., Guiraud, 1998). Triassic continental clastic systems sourced from uplifted Hercynian highs, flowed north-northeast through the Berkine Basin towards the peri-Tethys (Turner *et al*., 2001). In response to relative sea-level rise during the Middle Triassic, marine incursion occurred across Algeria, Tunisia and western Libya leading to the formation of a restricted Triassic salt basin (Turner & Sherif, 2007) in the northern portion of the Berkine and Oued Mya basins. Continued landward encroachment during the Late Triassic and Early Jurassic resulted in the progressive southward onlap of these successions onto older Paleozoic strata in the Illizi Basin (Galeazzi *et al*., 2010). On the southern flank of the Hoggar Massif, the Iullemmeden Basin was also a site of continental deposition during this time (Zanguina *et al.*, 1998).

Some interpretations consider that the Hoggar Massif remained an exposed high since the Hercynian orogeny until present-day (Fabre, 1976; Guiraud *et al.*, 2005; Liégeois *et al.*, 2005) while others interpret that deposition may have occurred over the Hoggar Massif during the Late Cretaceous–Early Eocene (Swezey, 2009; Rougier *et al.*, 2013). Evidence to support the latter interpretation are remnants of Jurassic to Cretaceous sediments that are widely preserved on the flanks of the uplifted Hoggar Massif. In the Serouenout area of northeastern Hoggar (Fig. 1), up to 350 m of poorly dated Upper Jurassic to Lower Cretaceous continental sandstones were deposited directly on basement (Bordet, 1954; Philippe *et al.*, 2003). The Serouenout sediments cover an area of ~6,000 km^2 with no indications of the basin limit (LeFranc & Guiraud, 1990). In

the Amguid area in the northern Hoggar (Fig. 1), Upper Cenomanian-Lower Turonian limestones unconformably overlie basement (Busson *et al.*, 1999). These outcrops lie along trend from the basement-controlled north-south oriented Amguid-El Biod High to the north (Fig. 1). This structure was the site of major transpressional deformation during the Late Neocomian-Middle Aptian Austrian event (Galeazzi *et al.*, 2010), and the presence of the Amguid limestones indicates at least partial inundation of this high during the Late Cretaceous. The short-lived Austrian tectonic event was characterized by strike-slip deformation along major intra-plate basement structures in North Africa, and was likely associated with the break-up of the Equatorial Atlantic and rifting in Central Africa (Guiraud *et al.*, 2005; Galeazzi *et al.*, 2010).

In general, the Cenozoic stratigraphy of the Sahara records a transition from early Cenozoic carbonate deposition to late Cenozoic siliciclastic deposition (Swezey, 2009). North of the Hoggar, outcrops of marine carbonates in the Tademaït region (Fig. 1) record deposition during the Late Cretaceous to Early Eocene. This sequence is capped by an unconformity, which is locally overlain by either Upper Eocene-Oligocene fluvial sandstones or Miocene-Pliocene fluvial sandstones and conglomerates (Swezey, 2009). In the Iullemmeden Basin, latest Paleocene to Eocene marine deposits are capped by continental Eocene to Miocene deposits; these sequences are separated by unconformities typically assigned to the Late Paleocene and Late Eocene-Oligocene (Kogbe, 1981; Burke & Gunnell, 2008). Clastic deposits of Late Eocene-Pliocene age in the Saharan region are collectively referred to as the "Continental Terminal" (Kilian, 1931; Lang *et al.*, 1990). Magmatic activity in the Hoggar area began at the Eocene-Oligocene boundary (~34 Ma) and has continued until the present (Girod, 1971; Aït Hamou *et al.*, 2000; Liégeois *et al.*, 2005; Azzouni-Sekkal *et al.*, 2007).

PREVIOUS STUDIES OF HOGGAR UPLIFT

Evidence of rock uplift, defined as vertical displacement of rock compared to a fixed frame of reference (England & Molnar, 1990), is observed in the core of the Hoggar, where the Precambrian basement attains average elevations of 1,000-1,500 m a.s.l. (Lesquer *et al.*, 1990), while locally reaching elevations of ~2,400 m a.s.l. in the Atakor region (Fig. 1) (Girod, 1971). The Upper Jurassic to Lower Cretaceous sandstones at Serouenout mostly occur at elevations

between 1,200 and 1,400 m a.s.l., although they can reach up to 1,700 m a.s.l. (Rougier, 2012). Sahagian (1988) used the distribution of Cenomanian shoreline deposits from the Trans-Sahara seaway preserved near the Hoggar to estimate that 2–3 km of uplift likely occurred in the area post-Cenomanian deposition. Volcanic centres, such as Mt. Tahat (2,909 m a.s.l.) in the Atakor area (Fig. 1), developed locally on top of the broader Hoggar swell during the Cenozoic.

Previous thermochronological analyses in the region have mainly focussed on outcrops from the Hoggar Massif (Carpena *et al.*, 1988; Meyer, 1990; Cavellec, 2006; Rougier *et al.*, 2013). Rougier *et al*. (2013) collected extensive apatite (U-Th)/He data and determined that the last phase of cooling and exhumation of the Hoggar Massif likely occurred during the Eocene. Apatite fission-track data from nearby basement outcrops in Aïr (Fig. 1; Cavellec, 2006) yield a central age of 44 ± 2.6 Ma, and linear cooling from peak temperatures >100°C in the early Cenozoic was interpreted based on thermal history modelling. Fission-track data from Carboniferous-Permian outcrops near Arlit (Fig. 1; Meyer, 1990) also yield similar Eocene-Oligocene ages (41-28 Ma), but track length data were not available to constrain thermal history models. Roberts & White (2010) also estimated that uplift of the Hoggar initiated during the Eocene based on modelling of longitudinal river profiles.

NEW THERMOCHRONOLOGICAL DATA FROM THE ILLIZI BASIN

Data Collection and Methodology

Thermal Maturity

Integration of thermal maturity and apatite fission-track data provides constraints on the maximum paleotemperature of the sedimentary fill, and the timing of the last major cooling event (e.g., Green & Duddy, 2012 and references therein). Vitrinite and bitumen reflectance and Rock-Eval data was collected from a suite of drill cuttings from Well A in the Illizi Basin (Fig. 1) in order to constrain the thermal maturity and peak paleotemperatures of Silurian to Carboniferous strata in the study area. Reflectance data was measured by two different laboratories (*KK: Keiraville Konsultants and EGS: Egs-ploration*). No sample count exceeds 14 measurements due to limited sample volume, and hence maturity estimates derived from the reflectance data must be treated with some caution. Only samples with > 5 measurements are

have been included in the study (Table 1). Bitumen reflectance was converted to vitrinite reflectance equivalent using a relationship from Schoenherr *et al.* (2007). The vitrinite reflectance data (and equivalents) were converted to an indicative estimate of maximum paleo-temperature using *Easy%Ro* (Sweeney & Burnham, 1990) and a fixed heating rate of 1°C/Myr. Rock-Eval pyrolysis data (Table 2) were screened according to the criteria of English *et al.* (2015) and Peters & Cassa (1994). The T_{max} to vitrinite reflectance conversion was adopted from Jarvie *et al.* (2001) and Peters *et al.* (2005).

Apatite Fission-Track

Ten sandstone-bearing intervals in Well A, ranging in age from Carboniferous (Namurian) to Ordovician, were also sampled for apatite-fission track analysis. Fission-track analysis was carried out by Geotrack International according to the sample preparation details described by Green (1986). Fission-track ages were determined by the external detector method (Gleadow, 1981) with zeta calibration (Hurford & Green, 1983) using dosimeter glass CN5 and a zeta of 392.9 ± 7.4 (*analyst MEM – Geotrack International*). Inverse modelling of the apatite fission-track data was utilised to constrain the range of possible time-temperature histories that are consistent with the measured data, and in particular to constrain (a) the timing and magnitude of maximum paleotemperature and (b) the timing and magnitude of the last major cooling event. Inverse modelling was carried out in *HeFTy v.1.8.2* (Ketcham, 2005) using the annealing kinetic model of Ketcham *et al.* (2007). Chlorine content (wt.%) was used as the kinetic parameter, and due to the generally low Cl contents (< 0.5 wt.%), each sample was modelled as a single population. C-axis projection was not used. The inverse models were run until 10,000 good paths were found. An acceptable and a good path were defined as having a goodness-of-fit (GOF) of > 0.05 and > 0.5 respectively according to the Kolmogorov-Smirnov test.

Results

Well A in the Illizi Basin penetrated 2118 m of Paleozoic stratigraphy ranging in age from Carboniferous (Namurian) to Ordovician. The results of the thermal maturity and apatite fission-track analysis are displayed in Tables 1-3 and graphically in Figure 2. The complete apatite fission-track dataset can be accessed in the Data Repository. The default profiles in Figure 2

illustrate predicted thermal maturity and apatite fission-track age if no additional burial is assumed.

Thermal Maturity

From the thermal maturity data (Fig. 2a), it is readily apparent that measured peak maturity values are consistently higher than what would be predicted from the present-day burial depth (the deposition of the preserved stratigraphy alone). The slope of the default maturity profile is broadly similar to the measured peak maturity profile, suggesting that the peak paleogeothermal gradient is likely similar to the present-day geothermal gradient. These observations confirm that this sedimentary sequence has been subjected to higher temperatures in the past, likely due to deeper burial, and that significant exhumation of the basin has occurred.

Apatite Fission-Track

The ten sandstone samples for fission-track analysis were derived from a limited volume of drill cuttings. Two of the samples yielded no apatite grains and the apatite yield was generally moderate in the other eight samples (grain counts ranged between 6 and 21). The P(χ2) test was applied to all samples, using a probability >5% as indicative of a homogeneous population (Galbraith, 1981). One sample (*GC1085-3*) produced a limited amount of data which failed the P(χ2) test, and is therefore excluded from further analysis here. Minor filtering in four of the remaining seven samples removed occasional spurious apatite grains with outlier chlorine contents or outlier fission track ages that appear to represent contamination. A summary of the final filtered dataset is presented in Table 3, but the data from the excluded grains from samples *GC1085-2*, *GC1085-6*, *GC1085-7* and *GC1085-8* are also provided in the Data Repository for completeness. The presented fission-track ages are pooled ages commonly used when P(χ2) > 5% (Galbraith & Laslett, 1993). The two samples with P(χ2) < 5% have central ages of 29.7±5.9 Ma (*GC1085-7*) and 8.5±2.4 Ma (*GC1085-10*). Only *GC1085-1* (Namurian) provided sufficient track length measurements (>100) to define a statistically meaningful track length distribution.

The measured apatite fission-track ages (Fig. 2b) for all samples, including the Carboniferous (Namurian) sample from a depth of only 180 m, are younger than their corresponding depositional ages, indicating that fission-track annealing has affected the entire preserved stratigraphic sequence, with increased annealing in deeper samples that have been

exposed to higher temperatures. The default profile illustrates the modelled vertical profile of apatite fission-track age assuming no additional burial beyond that preserved today. As chlorine content has been demonstrated to exert a systematic influence on annealing rates (Gleadow & Duddy, 1981; Green *et al.*, 1985, 1986), a fixed chlorine content of 0.1 wt.% has been assumed for the purposes of generating a vertical profile. Of the 93 apatite grains included in the analysis, 80% have chlorine contents less than or equal to 0.1 wt.%, and the average chlorine content is 0.07 wt.%. The default profile shows a characteristic "break-in-slope" (Fitzgerald & Gleadow, 1988, 1990; Fitzgerald *et al*., 1995; Green & Duddy, 2012) between present-day temperatures of ~60 and 90°C, while total annealing is expected below ~110 °C. The measured fission-track ages are routinely younger than the default profile, indicating this stratigraphic sequence has experienced hotter temperatures in the past. Samples from below ~1,000 m depth (Devonian, Silurian and Ordovician) are interpreted to have been totally annealed in the past (maximum temperatures > 110°C). Sixty-six apatite grains were analysed in these deeper samples (*GC1085-6*, *GC1085-7*, *GC1085-8*, *GC1085-9*, *GC1085-10*) yielding fission-track ages ranging from 73-0 Ma with an average of 17 Ma (see Data Repository); 96% of these grains yielded Eocene and younger fission-track ages. The shallower Carboniferous samples have only been partially annealed, and the fission-track age bears no relation to any specific thermal event.

Inverse Modelling of the Fission-Track Data

Inverse modelling was carried out in *HeFTy* to constrain the range of possible time-temperature histories that are consistent with the measured fission-track data (Ketcham, 2005). The initial (deposition) and final (present-day) conditions were defined in the model set-up, and additional constraint boxes were placed in temperature-time (T-t) space such that the inverse models would honour our general understanding of the burial history of the basin – i.e., pre-Hercynian burial, Hercynian exhumation, and post-Hercynian burial. Hercynian exhumation is modelled to be consistent with the maximum preserved thicknesses of Carboniferous strata in the eastern Illizi Basin (Galeazzi *et al*., 2010) and the Hercynian subcrop patterns observed immediately to the north of the study area (English *et al.*, 2016). Straight-line segments were modelled between the constraint boxes such that the inverse modelling would identify a series of relatively simple thermal histories that honour the fission-track data. The primary objective of the inverse modelling was to identify what constraints can be placed on the timing and

magnitude of maximum paleotemperature and also the timing and magnitude of the last major cooling event. Sample *GC1085-1* (Namurian) was selected for inverse modelling as this sample passed the P(χ2) test (11.7%) and provided the highest number of track length measurements (n = 106). As the number of measured track lengths is more limited in the deeper samples (Table 3), it was elected to combine the Devonian and Silurian samples *GC1085-6*, *GC1085-7* and *GC1085-8* to provide a more statistically meaningful sample set (n = 41) for inverse modelling. These samples were selected because they are from a narrow depth range (1385-1560 m), are at the lower temperature end of samples that have been fully annealed in the past (76-82°C present-day), and the combined fission-track age dataset also passes the P(χ2) test (5.2%).

Namurian Sample GC1085-1

The inverse modelling results for sample *GC1085-1* (Namurian) are presented in Figure 3a. The assumed timing constraints for the inverse modelling of this sample are as follows:

- A *pre-deposition* constraint (400-325 Ma) to account for inherited grains.
- The *depositional* constraint was set to approximate Namurian age (325-315 Ma) at 15-25°C surface temperature.
- The *post-deposition* constraints were defined on the basis of preserved stratigraphy and regional stratigraphic observations, and assume pre-Hercynian burial (300-260 Ma), Hercynian exhumation (260-160 Ma), and post-Hercynian reburial (180-0 Ma).
- Finally, the *present-day* temperature, based on downhole gauge temperature data from the well, defined the terminal conditions of the model.

The model was run until 10,000 good paths were identified. The vertices of the good paths (GOF > 0.5) are highlighted in purple, while the vertices of the acceptable paths (GOF > 0.05) are highlighted in green. The cloud of good path vertices during post-Hercynian reburial indicates that the maximum paleotemperature of the Namurian sample is likely to be in the 60-80°C range. Higher peak temperatures are allowable if maximum burial occurred during the Late Jurassic or Cretaceous as opposed to the Cenozoic (Fig. 3a). Hence, inverse modelling of the Namurian sample confirms that these strata reached maximum temperatures ~30-50°C higher than present-day, but does not provide clear constraints on the timing of maximum burial. The

best-fit of all the inverse model solutions is highlighted by the black line in the thermal history plot and reflects cooling from maximum temperatures in the Eocene (Fig. 3a). This inverse model solution provides a goodness-of-fit of 0.98 and 0.97 for the fission-track age and track length distribution respectively. This solution is non-unique and simply represents the best-fit of 10,000 different thermal histories that can provide a good fit to the measured data.

Silurian-Devonian Combined Sample GC1085-6,-7,-8

The inverse modelling results for the deeper combined samples *GC1085-6*, *GC1085-7* and *GC1805-8* (Devonian-Silurian) are presented in Figure 3b. The assumed timing constraints for the inverse modelling of this sample are as follows:

- A *depositional* constraint (423-400 Ma) at 5-15°C surface temperature. A pre-depositional constraint to allow for inherited grains is not required here as these samples have been fully annealed during burial.
- The *post-deposition* constraints were defined on the basis of preserved stratigraphy and regional stratigraphic observations, and assume pre-Hercynian burial (300-260 Ma), Hercynian exhumation (260-160 Ma), and post-Hercynian reburial (180-0 Ma).
- The *present-day* temperature defined the terminal conditions of the model.
- In addition, two *cooling* constraint boxes were added from 140-0 Ma at temperature intervals of 90-100°C and 70-85°C. These boxes are intermediate steps between post-Hercynian reburial and present-day conditions, but serve to capture the constraints that the fission-track data can place on the timing of cooling into the partial annealing zone during the latest phase of exhumation.

The model was again run until 10,000 good paths were identified. The cloud of purple good-path vertices (Fig. 3b) during post-Hercynian reburial confirms that the apatite fission-track data cannot provide any constraints on the thermal history above 110°C (due to total annealing), except confirming that cooling from maximum temperatures had to initiate before ~30 Ma. The cloud of good path vertices in the 90-100°C constraint box indicates that cooling through this temperature range likely occurred no earlier than ~50 Ma and no later than ~10 Ma – most likely during the 35-20 Ma window. Finally, the cloud of good path vertices in the 70-85°C constraint

box indicates that these samples reached temperatures close to present-day no earlier than ~30 Ma. Hence, inverse modelling of the Devonian-Silurian combined sample confirms that these strata reached higher temperatures in the total annealing zone in the past, and cooled by > 20°C during the Eocene or later to reach their present-day temperatures. The best-fit of all the inverse model solutions is highlighted by the black line in the thermal history plot and reflects cooling from maximum paleotemperatures in the Eocene (Fig. 3b). This inverse model solution provides a goodness-of-fit of 0.98 and 0.99 for the fission-track age and track length distribution respectively. This solution is non-unique and simply represents the best-fit of 10,000 different thermal histories that can provide a good fit to the measured data.

Summary

The inverse modelling confirms that deeper burial and hotter temperatures occurred in the study area in the past. The inverse modelling of the Namurian samples indicates maximum paleotemperatures ~30-50°C higher than present-day at some point during the Late Jurassic to Cenozoic (Fig. 3a). The inverse modelling of the deeper Devonian-Silurian samples indicates that at least 20°C of cooling occurred during the Eocene or later (Fig. 3b). Two main candidate tectonic events could have led to cooling from maximum burial temperature in this region (Galeazzi *et al*., 2010). **Model 1** is that exhumation from maximum burial conditions occurred during the Cenozoic and is related to uplift of the Hoggar Massif to the south of the study area. **Model 2** is that exhumation from maximum burial conditions occurred during the Middle Cretaceous and is related to possible uplift associated with the Austrian tectonic event. Model 2 would still require some Cenozoic cooling to honour the fission-track data from the deeper samples (Fig. 3b).

1D BURIAL HISTORY MODELLING

1D burial and thermal history modelling for Well A was carried out using the *Genesis* software (developed by Zetaware). Inputs for the thicknesses and lithologies of preserved and missing/eroded stratigraphy, present-day temperatures, and thermal maturity were based on well data and regional stratigraphic analysis (English *et al.*, 2016). The youngest preserved stratigraphy in Well A is Carboniferous, and missing/eroded stratigraphy assumptions were

reconstructed from younger preserved strata documented elsewhere in the Illizi and Berkine basins (Turner *et al.*, 2001; Yahi *et al*., 2001; Makhous & Galushkin, 2003; Turner & Sherif, 2007; Underdown *et al*., 2007; Dixon *et al*., 2010, Galeazzi *et al.*, 2010) and in outcrops (Swezey, 2009). Paleobathymetry was based on well-derived depositional facies and data from Yahi *et al.* (2001) from the Berkine Basin. The onset of post-Hercynian deposition in the study area is interpreted to have occurred in the Early Jurassic based on observed depositional edges within the Illizi Basin (Fig. 1). Paleolatitudes were used to approximate the paleo-surface temperature (Wygrala, 1989; Underdown, 2006).

Measured temperatures in Well A and 10 nearby wells indicate an average present-day geothermal gradient of 38°C/km (range 36-41°C/km), assuming an annual surface temperature of 22°C. The peak paleogeothermal gradient in the area is estimated to be ~37°C/km based on available thermal maturity data (English *et al.*, 2016). The calculated present-day basal heat flow is 65 mW/m^2, which is consistent with documented heat flows in the southern Illizi Basin (60 - 100 mW/m^2; Lesquer *et al.*, 1990). The basal heat flow was held constant through time in the *Genesis* models due to: (a) the similarity between the present-day geothermal gradient (38°C/km) and peak paleogeothermal gradients during maximum burial (~37°C/km), and (b) the absence of any major rifting event in the vicinity. Variations in heat flow have been assumed in some other studies in North Africa, such as in the Ahnet and Reggane basins (Fig. 1), where peak temperatures are related to a brief 'heat spike' or thermal anomaly at ~200 Ma, characterized by high peak paleogeothermal gradients (~60-80°C/km; Logan & Duddy, 1998) that are not observed in our Illizi Basin dataset.

Two independent 1D burial and thermal history models for Well A were constructed (Fig. 4) – one with maximum burial during the Cenozoic (Model 1) and one with maximum burial during the Middle Cretaceous (Model 2). Both thermal history models honour the preserved stratigraphy at Well A and the present-day temperature data. The post-Namurian depositional and erosional history was adjusted to calibrate to the available thermal maturity and apatite fission-track age data (Fig. 2). The modelled temperature-time (T-t) pathways for each layer in *Genesis* were imported into *HeFTy*, and a fixed chlorine content of 0.1 wt.% has been assumed for the purposes of generating a vertical profile of fission-track age for both Model 1 and Model 2 (Fig. 2b). These two vertical profiles are practically indistinguishable from each other, predict

a "break-in-slope" at much shallower depths than the default profile, and are more consistent with the measured fission-track age data. There is a small discrepancy in the shallower samples between the measured fission-track ages and the continuous profiles, and this may be because of (1) inherited tracks within these partially annealed grains or (2) a slightly higher Cl content. For example, the analysed grains in the shallowest Namurian sample have an average Cl content of 0.16 wt.%, and the modelled fission-track age for the actual grain population (blue squares – Model 1; red squares – Model 2) plots closer to the measured fission-track age (red circle) than the continuous profile assuming 0.1 wt.% Cl. Finally, both Model 1 and Model 2 were calibrated to the fission-track age and track length distributions for Namurian sample (*GC1085-1*) and the combined Devonian-Silurian samples (*GC1085-6*, *GC1085-7* and *GC1085-8*) via forward modelling of the associated T-t pathway in *HeFTy*. The forward modelling results for Model 1 and Model 2 are displayed in Figures 5 and 6 respectively. The goodness-of-fit (GOF) is greater than 0.85 in all cases except for the fission-track age in the Namurian sample where pre-depositional inheritance may be the cause of some additional variation.

Model 1 assumes additional post-Hercynian sedimentary burial throughout the Mesozoic with maximum burial in the Early Eocene (52 Ma), followed by (~1 km) exhumation during the Eocene-Miocene (Fig. 4a). Minor mid-Aptian exhumation (~25 m) is also included in this model to represent the Austrian unconformity. Model 2 assumes that maximum temperature occurs during the Aptian (124 Ma) followed by ~570 m of Austrian exhumation, with renewed Late Cretaceous and early Cenozoic burial, and ~840 m exhumation initiating during the Eocene (Fig. 4b). Both Model 1 and Model 2 honour the apatite fission-track and thermal maturity data for Well A (Figs. 2, 5 and 6).

TIMING OF MAXIMUM BURIAL IN THE ILLIZI BASIN

In the Illizi Basin, deformation and erosion associated with the Austrian tectonic event has been focussed along the north–south Amguid-El Biod fault trend at the western margin of the basin (Galeazzi *et al.*, 2010), while the more central parts of the Illizi Basin show less effect. Similarly, the Tihemboka Arch that defines the eastern boundary of the Illizi Basin does not show evidence of Austrian unroofing (Boote *et al.*, 2012). Within the study area, it is difficult to

comment with certainty on the magnitude of the Austrian erosional event due to the lack of sedimentary record. However, ~80 km north-northwest of Well A, pre- and post-Austrian strata at the Tin Fouyé Tabankort field (Chiarelli *et al.,* 1978; Fig. 1) do not display any significant angular discordance and are uniformly tilted northward together by a younger event. Based on this evidence, the preferred model for the study area involves maximum burial during the Cenozoic followed by exhumation and cooling in the Eocene-Miocene (Model 1). While the Mesozoic portion of the modelled thermal history solution is non-unique (i.e., Model 2 is also a possible valid model), the new dataset does require significant (0.5-1.0 km) Cenozoic exhumation in the study area to match the uniformly young fission-track ages in the deeper samples (e.g., Fig. 3b). The timing of the end of the exhumation cannot be definitively resolved, but a good fit to the fission-track data was achieved with significant exhumation ending during the Miocene. In the preferred Model 1, the total amount of Cenozoic exhumation at Well A in the Illizi Basin is estimated at ~1.0–1.1 km.

GEOMETRY AND MAGNITUDE OF HOGGAR UPLIFT AND EXHUMATION

Comparison with Regional Thermochronological Data

Previous apatite fission-track data over the Hoggar have provided widespread Mesozoic ages (Carpena *et al.*, 1988). New apatite fission-track data presented in this study from the Illizi Basin support other recent apatite (U-Th)/He thermochronologic data (Rougier *et al.*, 2013) and inverse modelling of longitudinal river profiles (Roberts & White, 2010), which indicate that the last major exhumation phase initiated during the Eocene. Rougier *et al.* (2013) reported apatite (U-Th)/He data from exposed basement samples adjacent to the Lower Cretaceous Serouenout deposits (Fig. 1), and interpreted that these rocks underwent post-depositional heating to 60-80°C, corresponding to 1-3 km of additional burial (assuming an Eocene geothermal gradient of 22-28°C/km and surface temperatures of 15-30°C), prior to exhumation. Using the maximum burial conditions assumed at Well A in the Illizi Basin (i.e., Eocene geothermal gradient of 36-41°C/km and surface temperature of 24°C), exhumation in the Serouenout area would correspond to ~0.9-1.6 km. It is possible that previously published Mesozoic apatite fission-track ages from outcrop samples of the Hoggar Massif (Carpena *et al.*, 1988) were only partially

annealed during subsequent Mesozoic-Cenozoic reburial, and hence the fission-track ages may not directly relate to any specific thermal event.

South of the Hoggar, in the Arlit area of Niger (Fig. 1), vitrinite reflectance and Rock-Eval pyrolysis data from the Carboniferous (Visean) Guézouman/Tarada Formation in the Tim Mersoï Basin indicate a thermal maturity of 0.66 R_o% and a T_{max} of 434°C at ~100m depth (sample 927/607; Forbes *et al.*, 1988). These measurements correspond to an estimated peak temperature of ~109°C using *Easy%Ro* (Sweeney & Burnham, 1990) and a fixed heating rate of 1°C/Myr. Rock-Eval pyrolysis data from the same formation in the Akouta area (sample CMK5; Salze, 1998), screened according to the criteria of English *et al.* (2015), yield a T_{max} of 430°C, and an equivalent R_o% of ~0.56 corresponds to an estimated peak temperature of ~95°C. Using the maximum burial conditions from Well A, these data suggest that the Visean formations reached maximum burial depths of ~1.7-2.3 km in the Tim Mersoï Basin. Apatite fission-track data from nearby basement outcrops in Aïr (Cavellec, 2006; Fig. 1) yield a central age of 44 ± 2.6 Ma and an average track length 12.56 ± 0.22 μm. Based on thermal history modelling, Cavellec (2006) interpreted a best-fit model with linear cooling from peak temperatures >100°C in the early Cenozoic. Fission-track data from Carboniferous-Permian outcrops near Arlit (Meyer, 1990) also yield similar Eocene-Oligocene ages (41-28 Ma), but track length data were not available to constrain thermal history models. Regionally, distinct Cenozoic exhumation has been interpreted in fission-track studies across the Ahnet Basin (Logan & Duddy, 1998), Tihemboka Arch (Glover, 1999; Boote *et al.*, 2012), and Al Qarqaf Arch (Underdown *et al.*, 2007), with only modest Cenozoic exhumation interpreted further north in the Berkine-Ghadames Basin (Underdown *et al.*, 2007) (Fig. 1).

In summary, these regional data confirm that a major Cenozoic cooling and exhumation event extended across the Hoggar region and into the surrounding sedimentary basins to the north and south. The preservation of a relatively complete Mesozoic-Cenozoic stratigraphic sequence in both the Berkine Basin (Galeazzi *et al.*, 2010) and the southern Iullemmeden Basin (Zanguina *et al.*, 1998) constrains the lateral extent of this exhumation event to the north and south respectively.

Geometry of the Hoggar Uplift

A regional schematic structural section has been constructed from the Berkine Basin in the north, across the Hoggar Massif, to the Iullemmeden Basin to the south, to define the geometry of the Hoggar uplift (Fig. 7). Following Rougier *et al.* (2013), we interpret that at least parts of the Hoggar Massif endured significant post-Hercynian Mesozoic and early Cenozoic reburial, although it remains unknown if this reburial affected the entire Hoggar region. Cenozoic rock uplift occurred across the Hoggar swell and surrounding basins over a distance >1,500 km from north to south, and uplift magnitudes within the core of the swell are in excess of 2 km (Fig. 7). These uplift estimates are consistent with ~1 km post-depositional burial of the Serouenout sandstones (at lower elevations), followed by uplift to their present-day elevations. Uplift magnitudes may be even greater in some local areas of the Hoggar such as Atakor (off-section from Fig. 7) where the Precambrian basement reaches elevations of ~2,400 m a.s.l. (Girod, 1971). Within the adjoining sedimentary basins, the magnitude of exhumation is interpreted to increase from the flanks towards the central part of the Hoggar uplift. The reduction in erosion within the core of the Hoggar (Fig. 7) may be due to the presence of more resistant crystalline basement compared to the sedimentary strata, or due to a reduction in fluvial erosion rates due to a smaller drainage area and lower discharge rates.

Driving Mechanisms for Uplift

The driving mechanisms for uplift of the Hoggar swell have been the subject of much debate (Liégeois *et al.*, 2005). A deep-mantle plume origin has been previously discounted based on the lack of an associated present-day thermal anomaly (Lesquer *et al.*, 1988; 1989), and the absence of expected evidence along the plate's projected path since 35 Ma (Liégeois *et al.*, 2005). As an alternative, Liégeois *et al.* (2005) proposed that edge-driven convection (King & Anderson, 1998), associated with changes in lithospheric thickness beneath the shield, may have facilitated asthenospheric mantle uprising and decompression melting during Eocene-Recent reactivation of Pan-African basement structures, linked to Africa-Eurasia collision to the north. Moucha & Forte (2011) and Jones *et al.* (2012) have both interpreted dynamic support for the Hoggar swell, indicating a role for underlying mantle convection. The data presented here indicates that the initiation of Cenozoic exhumation in the Illizi Basin, on the northern flank of the Hoggar swell, is coincident with the onset of intra-plate volcanism across a number of other North African magmatic provinces, including the Tibesti and Darfur districts (Wilson &

Guiraud, 1992; Wilson *et al.*, 1998; Liégeois *et al.*, 2005; Fig. 1), and is broadly co-eval with the onset of Africa-Eurasia collision during the Mid-Late Eocene (e.g. Frizon de Lamotte *et al.*, 2011). This collisional event resulted in inversion along the northwestern Atlas zone (Fig. 1), and concomitant minor angular unconformities can be observed in many North African sedimentary basins (e.g. Berkine, Oued Mya and Iullemmeden basins; Guiraud *et al.*, 2005; Lang *et al.*, 1990). However, the relationship between the Atlas event and the Hoggar uplift still remains unclear. Deposition of Upper Eocene-Pliocene sediments (the "Continental Terminal") across Saharan Africa (Kilian, 1931) may represent the onset of clastic sedimentation derived from the growing intracratonic swells, and the uplifting Atlasic belt to the north. Additionally, based on detrital zircon age-dating, the Hoggar region has been proposed as one of the possible source regions of reworked Oligocene to Miocene clastics of the Numidian Flysch deposited in the western Mediterranean (Thomas *et al.*, 2010).

CONCLUSIONS

This study quantifies the magnitude and timing of kilometre-scale uplift and exhumation of the Illizi Basin on the northern margin of the Hoggar swell. Integration with regional data indicates that the Cenozoic uplift event in the Hoggar region extended over a distance in excess of 1,500 km from north to south into the flanking basins, and the magnitude of rock uplift in the core of the swell is estimated to be in excess of 2 km. The timing of Cenozoic uplift is broadly coincident with magmatism on the Hoggar and other North African magmatic provinces, and with the onset of tectonic compression in the Atlasic belt to the north. Thermal history studies in sedimentary basins flanking other North African Cenozoic highs would help to constrain the true geometry and timing of these enigmatic rock uplifts, and help to unravel the continental-scale lithospheric and sub-lithospheric processes behind their genesis.

ACKNOWLEDGMENTS

We thank Petroceltic International, Sonatrach and Enel, for sponsoring this study and granting permission for publication. Additionally, we gratefully acknowledge Zhiyong He and Rich Ketcham for the generous donations of the *Genesis* and *HeFTy* software for this research. This manuscript has also benefitted from input by Dermot Corcoran, Sean McDade, Ian Duddy, Lorraine Eglinton and Sabine Cavellec in particular, and from constructive feedback from Cindy Ebinger, Yves Missenard and two anonymous reviewers. We also gratefully acknowledge Richard Dixon and Jake Hossack for sharing some of their insights on the evolution of the Hoggar swell.

CONFLICT OF INTEREST

No conflict of interest declared.

REFERENCES

ACHECHE, M.H., M'RABET, A., GHARIANI, H., OUAHCHI, A. & MONTGOMERY, S.L. (2001) Ghadames basin, southern Tunisia: A reappraisal of Triassic reservoirs and future prospectivity. *AAPG Bull.*, **85**, 765–780.

AÏT HAMOU, F., DAUTRIA, J.M., CANTAGREL, J.M., DOSTAL, J. & BRIQUEU, L. (2000) Nouvelles données géochronologiques et isotopiques sur le volcanisme cénozoïque de l'Ahaggar (Sahara algérien): Des arguments en faveur d'un panache. *Comptes Rendus de l'Académie des Sciences de Paris*, **330**, 829–836.

AL-HAJRI, Y., WHITE, N. & FISHWICK, S. (2009) Scales of transient convective support beneath Africa. *Geology*, **37**, 883–886.

ALIEV, M., AÏT LAOUSSINE, N., AVROV, V., ALEKSINE, G., BAROULINE, G., LAKOVLEV, B., KORJ, M., KOUVYKINE, J., MAKAROV, V., MAZANOV, V., MEDVEDEV, E., MKRTCHIANE, O., MOUSTAFINOV, R., ORIEV, L., OROUDJEVA, D., OULMI, M. & SAÏD, A. (1971) *Geological structures and estimation of oil and gas in the Sahara in Algeria*. Altamira-Rotopress, S.A., Spain, 265 pp.

AZZOUNI-SEKKAL, A., BONIN, B., BENHALLOU, A., YAHIAOUI, R. & LIÉGEOIS, J.P. (2007) Cenozoic alkaline volcanism of the Atakor massif, Hoggar, Algeria. In: *Cenozoic volcanism in the Mediterranean area* (Ed. by L. Beccaluva, G. Bianchini & M. Wilson), *Geol. Soc. Am. Spec. Paper*, **418**, 321–340.

BECCALUVA, L., AZZOUNI-SEKKAL, A., BENHALLOU, A., BIANCHINI, G., ELLAM, R.M., MARZOLA, M., SIENA, F. & STUART, F.M. (2007) Intracratonic asthenosphere upwelling and lithosphere rejuvenation beneath the Hoggar swell (Algeria): Evidence from HIMU metasomatised lherzolite mantle xenoliths. *Earth Planet. Sci. Lett.*, **260**, 482–494.

BEUF, S., BIJU-DUVAL, B., DE CHARPAL, O., ROGNON, P., GARIEL, O. & BENNACEF, A. (1971) *Les grès du Paléozoïque inférieur au Sahara*. Publications de l'Institut Français du Pétrole, Coll. Science et Technique du Pétrole **18**, Paris, 464 pp.

BOOTE, D. (2013) The 'Austrian Event' of the Afro-Arabian Plate and its influence upon Cretaceous petroleum systems. *AAPG European Regional Conference*, Barcelona, Spain, April 8-10, 2013.

BOOTE, D.R.D., CLARK-LOWES, D.D. & TRAUT, M.W. (1998) Palaeozoic petroleum systems of North Africa. In: *Petroleum geology of North Africa* (Ed. by D.S. MacGregor, R.T.J. Moody & D.D. Clark-Lowes), *Geol. Soc. Lond., Spec. Publ.*, **132**, 7–68.

BOOTE, D.R.D., DARDOUR, A., GREEN, P.F., SMEWING, J.D. & VAN HOEFLAKEN, F. (2012) Burial and unroofing history of the base Tanezzuft 'hot' shale source rock, Murzuk basin, SW Libya: New AFTA constraints from basin margin outcrops. *Geol. South. Libya*, **2**, 21–36.

BORDET, P. (1954) La série de Serouenout (Ahaggar oriental) est d'âge "Continental Intercalaire" (Crétacé Moyen). *Comptes Rendus de l'Académie des Sciences*, **238**, 500–503.

BRAUN, J. (2010) The many surface expressions of mantle dynamics. *Nature Geosc.*, **3**, 825–833.

BURKE, K. (1996) The African plate. *South Afr. J. Geol.*, **99**, 341–409.

BURKE, K. & GUNNELL, Y. (2008) The African erosion surface: A continental-scale synthesis of geomorphology, tectonics and environmental change over the past 180 million years. Geological Society of America Memoirs, **201**, 1-66.

BUROLLET, P., MUGNIOT, J. & SWEENEY, P. (1978) The geology of the Pelagian block: the margins and basins off southern Tunisia and Tripolitania. In: *The Western Mediterranean* (Ed. by A. Nairn, W. Kanes & F. Stehli), *The Ocean Basins and Margins, Springer*, 331–359.

BUSSON, G., DHONDT, A., AMÉDRO, F., NÉRAUDEAU, D. & CORNÉE, A. (1999) La grande transgression du Cénomanien supérieur-Turonien inférieur sur la Hamada de Tinrhert (Sahara algérien): Datations biostratigraphiques, environnement de dépôt et comparaison d'un témoin épicratonique avec les séries contemporaines à matière organique du Maghreb. *Cret. Res.*, **20**, 29–46.

CARPENA, J., KIENAST, J., OUZEGANE, K. & JEHANNO, C. (1988) Evidence of the contrasted fission track clock behavior of the apatites from In Ouzzal carbonatites (northwest Hoggar): The low-temperature thermal history of an Archean basement. *Geol. Soc. Am. Bull.*, **100**, 1237–1243.

CAVELLEC, S. (2006) Evolution diagénétique du basin de Tim Mersoï et conséquences pour la génèse des minéralisations uranifères dans les formations carbonifères du Guezouman et du Tarat (district Arlit-Akokan, Niger). PhD thesis, Université du Paris-Sud, Paris, France.

CHOUBERT, A. & FAURE-MURET, A. (1990) *International geological map of Africa*. CGMW (Commission of the Geological Map of the World), UNESCO, Paris, France, scale 1:5,000,000, 6 sheets.

DAUTRIA, J.M. & LESQUER, A. (1989) An example of the relationship between rift and dome: recent geodynamic evolution of the Hoggar Swell and of its nearby regions (Central Sahara, Southern Algeria and Eastern Niger). *Tectonophysics*, **163**, 45–61.

DIXON, R.J., MOORE, J.K.S., BOURNE, M., DUNN, E., HAIG, D.B, HOSSACK, J., ROBERTS, N., PARSONS, T. & SIMMONS, C.J. (2010) Integrated petroleum systems and play fairway analysis in a complex Palaeozoic basin: Ghadames-Illizi Basin, North Africa. In: *Petroleum geology: From mature basins to new frontiers* (Ed. by B.A. Vining & S.C. Pickering), *Geol. Soc. Lond., Petrol. Geol. Conf. Series*, **7**, 735–760.

ENGLAND, P. & MOLNAR, P. (1990) Surface uplift, uplift of rocks, and exhumation of rocks. *Geology*, **18**, 1173–1177.

ENGLISH, J.M., LUNN, G.A., FERREIRA, L. & YACU, G. (2015) Geologic evolution of the Iraqi Zagros, and its influence on the distribution of hydrocarbons in the Kurdistan region. *AAPG Bull.*, **99**, 231–272.

ENGLISH, K.L., REDFERN, J., CORCORAN, D.V., ENGLISH, J.M. & YAHIA CHERIF, R. (2016) Constraining burial history and petroleum charge in exhumed basins: new insights from the Illizi Basin, Algeria. *AAPG Bull.,* **100**, XXX–XXX.

FABRE, J. (1976) *Introduction à la géologie du Sahara algérien et des régions voisines*. Sociétié Nationale d'Édition et de Diffusion, Algiers, Algeria, 422 pp.

FITZGERALD, P.G. & GLEADOW, A.J.W. (1988) Fission-track geochronology, tectonics and structure of the Transantarctic Mountains in Northern Victoria Land, Antarctica. *Chem. Geol.*, **73**, 169–198.

FITZGERALD, P.G. & GLEADOW, A.J.W. (1990) New approaches in fission track geochronology as a tectonic tool: Examples from the Transantarctic Mountains. *Nucl. Tracks Radiat. Meas.*, **17**, 351-357.

FITZGERALD P.G., SORKHABI, R.B., REDFIELD, T.F. & STUMP, E. (1995) Uplift and denudation of the central Alaska Range: A case study in the use of apatite fission track thermochronology to determine absolute uplift parameters. *J. Geophy. Res.,* **100**, 20175-20191.

FORBES, P., LANDAIS, P., BERTRAND, P., BROSSE, E., ESPITALIÉ, J. & YAHAYA, M. (1988) Chemical Transformations of Type-III Organic Matter Associated with the Akouta Uranium Deposit (Niger): Geological Implications. *Chem. Geol.*, **71**, 267–282.

FRIZON DE LAMOTTE, D., RAULIN, C., MOUCHOT, N., WROBEL-DAVEAU, J.C., BLANPIED, C. & RINGENBACH, J.C. (2011) The southernmost margin of the Tethys realm during the Mesozoic and Cenozoic: Initial geometry and timing of the inversion processes. *Tectonics*, **30**, TC3002.

GALBRAITH, R.F. (1981) On statistical models for fission-track counts. *Math. Geol.*, **13**, 471–478.

GALBRAITH, R.F. & LASLETT, G.M. (1993) Statistical models for mixed fission-track ages. *Nucl. Tracks Radiat. Meas.*, **21**, 459–470.

GALEAZZI, S., POINT, O., HADDADI, N., MATHER, J. & DRUESNE, D. (2010) Regional geology and petroleum systems of the Illizi–Berkine area of the Algerian Saharan Platform: An overview. *Mar. Petrol. Geol.*, **27**, 143–178.

GENIK, G.J. (1993) Petroleum geology of Cretaceous–Tertiary rift basins in Niger, Chad, and Central African Republic. *AAPG Bull.*, **77**, 1405–1434.

GIROD, M. (1971) *Le massif volcanique de l'Atakor (Hoggar, Sahara Algérien). Étude pétrographique, structurale et volcanologique*. Centre de Recherches sur les Zones Arides, série Géologie **12**, Éditions du Centre National de la Recherche Scientifique, Paris, France, 158 pp.

GLEADOW, A.J.W. (1981) Fission-track dating methods: What are the real alternatives? *Nucl. Tracks*, **5**, 3–14.

GLEADOW, A.J.W. & DUDDY, I.R. (1981) Fission track analysis: a new tool for the evaluation of thermal histories and hydrocarbon potential. *Aust. Petrol. Expl. Assoc. J.,* **23**, 93-102.

GLOVER, R.T. (1999) Aspects of intraplate deformation in Saharan Cratonic Basins. PhD thesis, University of Wales, Aberystwyth, United Kingdom.

GREEN, P.F. (1986) On the thermo-tectonic evolution of Northern England: evidence from fission-track analysis. *Geol. Mag.*, **123**, 493–506.

GREEN, P. & DUDDY, I.R. (2012) Thermal history reconstruction in sedimentary basins using apatite fission-track analysis and related techniques. In: *Analyzing the thermal history of sedimentary basins: Methods and case studies* (Ed. by N.B. Harris & K.E. Peters), *Soc. Sed. Geol., Spec. Publ.*, **103**, 65–104.

GREEN, P.F., DUDDY, I.R., GLEADOW, A.J.W., TINGATE, P.R. & LASLETT, G.M. (1985) Fission-track annealing in apatite: track length measurements and the form of the Arrhenius plot. *Nucl. Tracks*, **10**, 323–328.

GREEN, P.F., DUDDY, I.R., GLEADOW, A.J.W., TINGATE, P.R. & LASLETT, G.M. (1986) Thermal annealing of fission tracks in apatite: 1. A qualitative description. *Chem. Geol.*, **59**, 237–253.

GUIRAUD, R. (1998) Mesozoic rifting and basin inversion along the northern African Tethyan margin: an overview. In: *Petroleum geology of North Africa* (Ed. by D.S. MacGregor, R.T.J. Moody & D.D. Clark-Lowes), *Geol. Soc. Lond., Spec. Publ.*, **132**, 217–229.

GUIRAUD, R., BOSWORTH, W., THIERRY, J. & DELPLANQUE, A. (2005) Phanerozoic geological evolution of northern and central Africa: An overview. *J. Afr. Earth Sci.*, **43**, 83–143.

HOLMES, A. (1944) *Principles of Physical Geology*. Thomas Nelson & Sons Ltd., Edinburgh, United Kingdom, 532 pp.

HURFORD, A.J. & GREEN, P.F. (1983) The zeta age calibration of fission-track dating. *Chem. Geol.*, **41**, 285–317.

JARVIE, D., CLAXTON, B., HENK, B. & BREYER, J. (2001) Oil and shale gas from the Barnett Shale, Fort Worth Basin, Texas. *AAPG Annual Meeting Program*, **10**, A100.

JONES, S.M., LOVELL, B. & CROSBY, A.G. (2012) Comparison of modern and geological observations of dynamic support from mantle convection. *J. Geol. Soc. Lond.*, **169**, 745–758.

KETCHAM, R.A. (2005) Forward and inverse modeling of low-temperature thermochronometry data. *Rev. Min. & Geochem.*, **58**, 275–314.

KETCHAM, R.A., CARTER, A., DONELICK, R.A., BARBARAND, J. & HURFORD, A.J. (2007) Improved modelling of fission-track annealing in apatite. *Am. Mineralogist*, **92**, 799–810.

KILIAN, C. (1931) Des principaux complexes continentaux du Sahara. *Comptes Rendus sommaire de la Societé Géologique de la France*, **9**, 109–111.

KING, S.D. & ANDERSON, D.L. (1998) Edge-driven convection. *Earth Planet. Sci. Lett.*, **160**, 289–296.

KOGBE, C.A. (1981) Cretaceous and Tertiary of the Iullemmeden Basin in Nigeria (West Africa). *Cret. Res.*, **2**, 129-186.

LANG, J., KOGBE, C., ALIDOU, S., ALZOUMA, K.A., BELLION, G., DUBOIS, D., DURAND, A., GUIRAUD, R., HOUESSOU, A., DE KLASZ, I., ROMANN, E., SALARD-CHEBOLDAEFF, M. & TRICHET, J. (1990) The continental terminal in West Africa. *J. Afr. Earth Sci.*, **10**, 79–99.

LEFRANC, J.P. & GUIRAUD, R. (1990) The continental intercalaire of northwestern Sahara and its equivalents in the neighbouring regions. *J. Afr. Earth Sci.*, **10**, 27–77.

LESQUER, A., BOURMATTE, A. & DAUTRIA, J.M. (1988) Deep structure of the Hoggar domal uplift (central Sahara, south Algeria) from gravity, thermal and petrological data. *Tectonophysics*, **152**, 71–87.

LESQUER, A., BOURMATTE, A., LY, S. & DAUTRIA, J.M. (1989) First heat flow determination from the Central Sahara: Relationship with the Pan-African belt and Hoggar domal uplift. *J. Afr. Earth Sci.*, **9**, 41–49.

LESQUER, A., TAKHERIST, D., DAUTRIA, J.M. & HADIOUCHE, O. (1990) Geophysical and petrological evidence for the presence of an "anomalous" upper mantle beneath the Sahara basins (Algeria). *Earth Planet. Sci. Lett.*, **96**, 407–418.

LIÉGEOIS, J.P., BENHALLOU, A., AZZOUNI-SEKKAL, A., YAHIAOUNI, R. & BONIN, B. (2005) The Hoggar swell and volcanism: Reactivation of the Precambrian Tuareg shield during Alpine convergence and West African Cenozoic volcanism. In: *Plates, plumes and paradigms* (Ed. by

G.R. Foulger, J.H. Natland, D.C. Presnall & D.L. Anderson), *Geol. Soc. Am. Spec. Paper*, **388**, 379–400.

LOGAN, P. & DUDDY, I. (1998) An investigation of the thermal history of the Ahnet and Reggane basins, central Algeria, and the consequences for hydrocarbon generation and accumulation. In: *Petroleum geology of North Africa* (Ed. by D.S. MacGregor, R.T.J. Moody & D.D. Clark-Lowes), *Geol. Soc. Lond., Spec. Publ.*, **132**, 131–155.

MAKHOUS, M. & GALUSHKIN, Y.I. (2003) Burial history and thermal evolution of the northern and eastern Saharan basins. *AAPG Bull.,* **87**, 1623-1651.

MEYER, A.J. (1990) Les traces de fission dans l'apatite : Etude expérimentale et application à l'histoire thermique de bassins sédimentaires. PhD thesis, Institut National Polytechnique de Lorraine, Nancy, France.

MOUCHA, R. & FORTE, A.M. (2011) Changes in African topography driven by mantle convection. *Nature Geosci.*, **4**, 707–712.

PETERS, K.E. & CASSA, M.R. (1994) Applied source rock geochemistry. In: *The petroleum system – From source to trap* (Ed. by L.B. Magoon & W.G. Dow), *AAPG Memoir*, **60**, 93–120.

PETERS, K.E., WALTERS, C.C. & MOLDOWAN, J.M. (2005) *The Biomarker Guide, Volume 1: Biomarkers and Isotopes in the Environment and Human History*. Cambridge University Press, Cambridge, UK, 492 pp.

PHILIPPE, M., CUNY, G., BAMFORD, M., JAILLARD, E., BARALE, G., GOMEZ, B., OUAJA, M., THÉVENARD, F., THIÉBAUT, M. & VON SENGBUSCH, P. (2003) The palaeoxylological record of *Metapodocarpoxylon libanoticum* (Edwards) Dupéron-Laudoueneix et Pons and the Gondwana Late Jurassic–Early Cretaceous continental biogeography. *J. Biogeog.*, **30**, 389–400.

ROBERTS, G.G. & WHITE, N. (2010) Estimating uplift rate histories from river profiles using African examples. *J. Geophys. Res.*, **115**, B02406.

ROUGIER, S. (2012) Interactions lithosphere-asthenosphere et mouvements verticaux: Le cas du Massif du Hoggar. PhD thesis, Universite Paris-Sud, Paris, France.

ROUGIER, S., MISSENARD, Y., GAUTHERON, C., BARBARAND, J., ZEYEN, H., PINNA, R., LIÉGEOIS, J.P., BONIN, B., OUABADI, A., EL-MESSAOUD DERDER, M. & FRIZON DE LAMOTTE, D. (2013) Eocene exhumation of the Tuareg Shield (Sahara Desert, Africa). *Geology*, **41**, 615–618.

SAHAGIAN, D. (1988) Epeirogenic motions of Africa as inferred from Cretaceous shoreline deposits. *Tectonics*, **7**, 125–138.

SALZE, D. (2008) Etude des interactions entre uranium et composés organiques dans les systèmes hydrothermaux. PhD thesis, Université Henri Poincaré, Nancy, France.

SCHOENHERR, J., LITTKE, R., URAI, J., KUKLA, P. & RAWAHI, Z. (2007) Polyphase thermal evolution in the Infra-Cambrian Ara Group (South Oman Salt Basin) as deduced by maturity of solid reservoir bitumen. *Org. Geochem.*, **38**, 1293–1318.

SWEENEY, J. & BURNHAM, A. (1990) Evaluation of a simple model of vitrinite reflectance based on chemical kinetics. *AAPG Bull.*, **74**, 1559–1570.

SWEZEY, C.S. (2009) Cenozoic stratigraphy of the Sahara, Northern Africa. *J. Afr. Earth Sci.*, **53**, 89–121.

THOMAS, M.F.H., BODIN, S., REDFERN, J. & IRVING, D.H.B. (2010) A constrained African craton source for the Cenozoic Numidian Flysch: Implications for the paleogeography of the western Mediterranean basin. *Earth Sci. Reviews.*, **101**, 1–23.

TURNER, P., PILLING, D., WALKER, D., EXTON, J., BINNIE, J. & SABAOU, N (2001) Sequence stratigraphy and sedimentology of the late Triassic TAG-I (Blocks 401/402, Berkine Basin, Algeria). *Mar. Petrol. Geol.,* **18**, 959-981.

TURNER, P. & SHERIF, H. (2007) A giant Late Triassic-Early Jurassic evaporitic basin on the Saharan Platform, North Africa. In: *Evaporites through space and time* (Ed. by B.C. Schreiber, S. Lugli & M. Babel), *Geol. Soc. Lond., Spec. Publ.*, **285**, 87–105.

UNDERDOWN, R. (2006) An integrated basin modelling study of the Ghadames Basin, North Algeria. PhD thesis, University of Manchester, United Kingdom.

UNDERDOWN, R., REDFERN, J. & LISKER, F. (2007) Constraining the burial history of the Ghadames basin, North Africa: an integrated analysis using sonic velocities, vitrinite reflectance and apatite fission track ages. *Basin Res.*, **19**, 557–578.

WILSON, M. & GUIRAUD, R. (1992) Magmatism and rifting in Western and Central Africa, from Late Jurassic to Recent times. *Tectonophysics*, **213**, 203–225.

WILSON, M., GUIRAUD, R., MOREAU, C. & BELLION, Y.J.C. (1998) Late Permian to Recent magmatic activity on the African-Arabian margin of Tethys. In: *Petroleum geology of North Africa* (Ed. by D.S. MacGregor, R.T.J. Moody & D.D. Clark-Lowes), *Geol. Soc. Lond., Spec. Publ.*, **132**, 231–263.

WYGRALA, B.P. (1989) Integrated study of an oil field in the southern Po basin, northern Italy. PhD thesis, Köln University, Research Centre Jülich, Germany.

YAHI, N., SCHAEFER, R.G. & LITTKE, R. (2001) Petroleum generation and accumulation in the Berkine Basin, eastern Algeria. *AAPG Bull.*, **85**, 1439–1467.

YARMOLYUK, V.A. & KUZNETSOV, Y.Y. (1977) *Geological map of Africa*. Ministry of Geology of the USSR, Moscow, Russia, scale 1:5,000,000, 9 sheets.

ZANGUINA, M., BRUNETON, A. & GONNARD, R. (1998) An introduction to the petroleum potential of Niger. *J. Petrol. Geol.*, **21**, 83–103.

List of Tables

List of Figures

and show a trend of decreasing fission-track age with depth due to greater degree of annealing. The default profile illustrates the predicted fission-track ages for apatites with 0.1 wt.% chlorine content if no additional burial is assumed. The measured fission-track ages are routinely younger than the default profile, consistent with the interpretation that this stratigraphic sequence has experienced hotter temperatures in the past. The predicted profile from the preferred Well A model (Model 1), also assuming a chlorine content of 0.1 wt.%, provides a much better fit to the data. Samples with higher chlorine contents will be more resistant to annealing for a given thermal history. Fission-track modelling was carried out with *HeFTy* using the annealing kinetics of Ketcham *et al.* (2007).

Figure 3: Inverse modelling of the (A) Namurian sample *GC1085-1* and the (B) deeper Devonian-Silurian sample combined from *GC1085-6*, *GC1085-7* and *GC1085-8.* The models were run until 10,000 good paths were identified. The vertices of the good paths (GOF > 0.5) are highlighted in purple, while the vertices of the acceptable paths (GOF > 0.05) are highlighted in green. The best-fit of all the inverse model solutions is highlighted by the black line in the thermal history plot. These solutions are non-unique and simply represent the best-fit of 10,000 different thermal histories that can provide a good fit to the measured data.

Figure 4: 1D thermal history models for Well A calibrated to thermal maturity and fission-track data. (A) Model 1 assumes maximum burial during the Eocene. (B) Model 2 assumes maximum burial during the Middle Cretaceous at the Austrian tectonic event. Additionally, slightly more Carboniferous deposition in Model 2 (50m) with 25m less Hercynian erosion was required to best match maturity. While these solutions are non-unique, the new data require significant additional burial to match the peak paleotemperature constraints, followed by the onset of significant exhumation during the Eocene. Thermal history modelling was carried out using *Genesis.*

Figure 5: Temperature-time (T-t) histories from Model 1 for (A) the Namurian sample (*GC1085-1*) and (B) the combined Devonian-Silurian samples (*GC1085-6*, *GC1085-7* and *GC1085-8*) exported from *Genesis* into *HeFTy*. Forward modelling of the T-t pathways in *HeFTy* provide a very good fit (GOF > 0.85) for the track length distribution in both samples and for the fission-track age in the Devonian-Silurian samples. The goodness-of-fit is lower for the

fission-track age in the Namurian sample and this may be due to preservation of pre-depositional inheritance as this sample was not fully annealed during burial.

Figure 6: Temperature-time (T-t) histories from Model 2 for (A) theNamurian sample (*GC1085-1*) and (B) the combined Devonian-Silurian samples (*GC1085-6*, *GC1085-7* and *GC1085-8*) exported from *Genesis* into *HeFTy*. Forward modelling of the T-t pathways in *HeFTy* provide a very good fit (GOF > 0.85) for the track length distribution in both samples and for the fission-track age in the Devonian-Silurian samples. The goodness-of-fit is lower for the fission-track age in the Namurian sample and this may be due to preservation of pre-depositional inheritance as this sample was not fully annealed during burial.

Figure 7: Schematic structural section across the Hoggar Massif from the Berkine Basin in the north to the Iullemmeden Basin in the south (see transect in Fig. 1). Note that the Hoggar had an earlier history of uplift with significant erosion of the Paleozoic sequence during the Hercynian orogeny. Preserved thicknesses are taken from well data (Illizi-Berkine), geology maps and published cross sections (Iullemmeden Basin, Zanguina *et al.*, 1998; Genik, 1993; Dautria & Lesquer, 1989). The eroded stratigraphy of the Tim Mersoï, Hoggar and Illizi regions is projected above the present day surface and calibrated to ~ 1 km of exhumation in Well A, ~ 0.9-1.6 km exhumation in the Serouenout area, and peak burial depths of ~ 1.7-2.3 km for the Visean projected from the Arlit area. Note that the actual magnitude of exhumation in Arlit/Arouta (on the flank of Aïr; Fig. 1) is higher than where it is projected on this section (Carboniferous at surface). Regional data suggests portions of the Central Hoggar may have been inundated with > 1 km of Upper Cretaceous – lower Paleogene sediment. Cenozoic rock uplift across the Hoggar occurred over a distance of >1,500 km from north to south, as indicated by the tilted Cenozoic stratigraphy in the Berkine and Iullemmeden basins. The magnitude of rock uplift, as opposed to exhumation, reaches in excess of 2 km within the core of the Hoggar Massif. Deposition of Upper Eocene-Pliocene sediments (the “Continental Terminal”) across Saharan Africa (Kilian, 1931) may represent the onset of clastic sedimentation derived from the growing intracratonic swells.

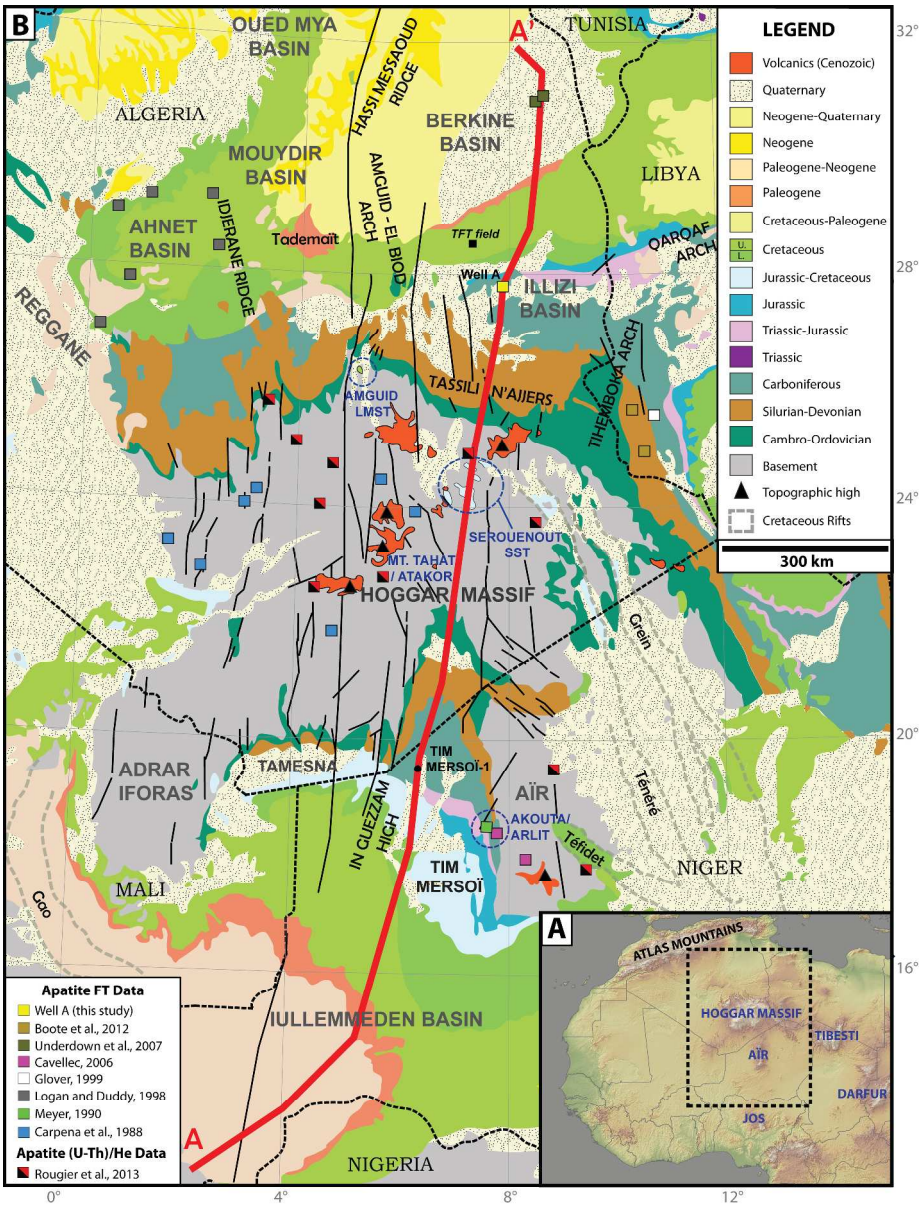

Figure 1: (A) Topographic map of North Africa showing the Hoggar and Aïr massifs, and location of other Cenozoic volcanic areas including Tibesti and Darfur (Lesquer et al., 1988). (B) Simplified geology map of the Hoggar and Aïr massifs and flanking sedimentary basins (adapted from Yarmolyuk & Kuznetsov, 1977; Choubert & Faure-Muret, 1990; LeFranc & Guiraud, 1990; Genik, 1993). Dated Mesozoic sediments that unconformably overlie basement (Serouenout and Amguid localities) are highlighted. Preserved Cenozoic sediments described in the text are located in the Tademaït region. Location of Tin Fouyé Tabankort field (TFT) is noted where post-Hercynian deposits are preserved. Other information includes locations of thermal maturity data (Well A, Akouta and Arlit), new apatite fission track data (Well A), and published apatite thermochronology sample sites (Hoggar, Aïr, Ahnet, Tihemboka, Qarqaf Arch). Note that Logan and Duddy (1998) study includes both apatite fission track, and zircon fission track analysis. Refer to Figure 7 for illustration of the north-south transect (A-A') across the Hoggar Massif into the flanking basins.

Figure 2

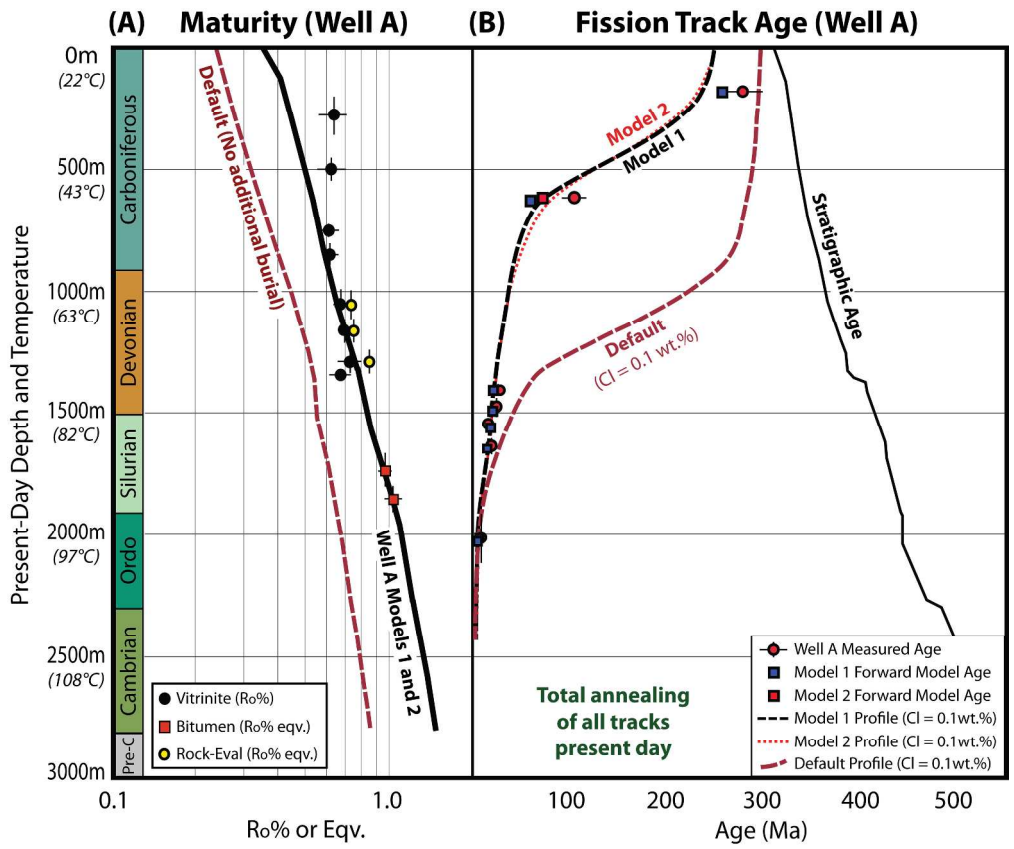

Figure 2: (A) Actual Well A thermal maturity data (black circles) versus modelled thermal maturity profile (black line) according to depth. Models 1 and 2 maturity profiles are identical. The default profile illustrates predicted maturity if no additional burial is assumed. Present-day thermal maturity is higher than what would be expected from current burial depths (default maturity profile shown by dashed red line) indicating that these rocks have been hotter in the past. (B) Actual Well A fission-track ages (red circles) versus modelled fission-track ages (blue squares, Model 1; red squares, Model 2) according to depth. Most modelled fission-track ages for the actual grain populations for Models 1 and 2 overlie except for GC1085-2 (Visean). All samples provide fission-track ages that are younger than their corresponding depositional ages, and show a trend of decreasing fission-track age with depth due to greater degree of annealing. The default profile illustrates the predicted fission-track ages for apatites with 0.1 wt.% chlorine content if no additional burial is assumed. The measured fission-track ages are routinely younger than the default profile, consistent with the interpretation that this stratigraphic sequence has experienced hotter temperatures in the past. The predicted profile from the preferred Well A model (Model 1), also assuming a chlorine content of 0.1 wt.%, provides a much better fit to the data. Samples with higher chlorine contents will be more resistant to annealing for a given thermal history. Fission-track modelling was carried out with HeFTy using the annealing kinetics of Ketcham et al. (2007).

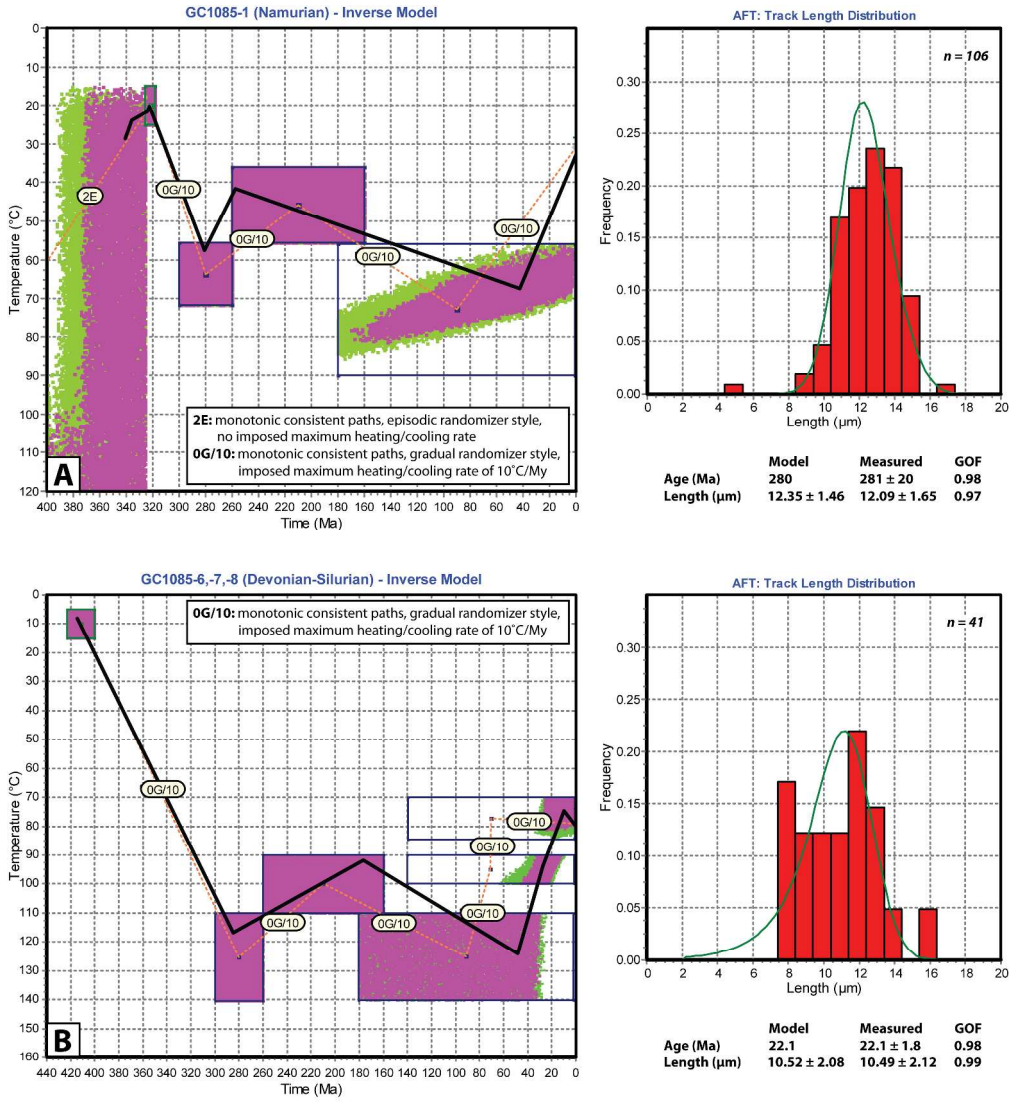

Figure 3

Figure 3: Inverse modelling of the (A) Namurian sample GC1085-1 and the (B) deeper Devonian-Silurian sample combined from GC1085-6, GC1085-7 and GC1085-8. The models were run until 10,000 good paths were identified. The vertices of the good paths (GOF > 0.5) are highlighted in purple, while the vertices of the acceptable paths (GOF > 0.05) are highlighted in green. The best-fit of all the inverse model solutions is highlighted by the black line in the thermal history plot. These solutions are non-unique and simply represent the best-fit of 10,000 different thermal histories that can provide a good fit to the measured data.

Figure 4

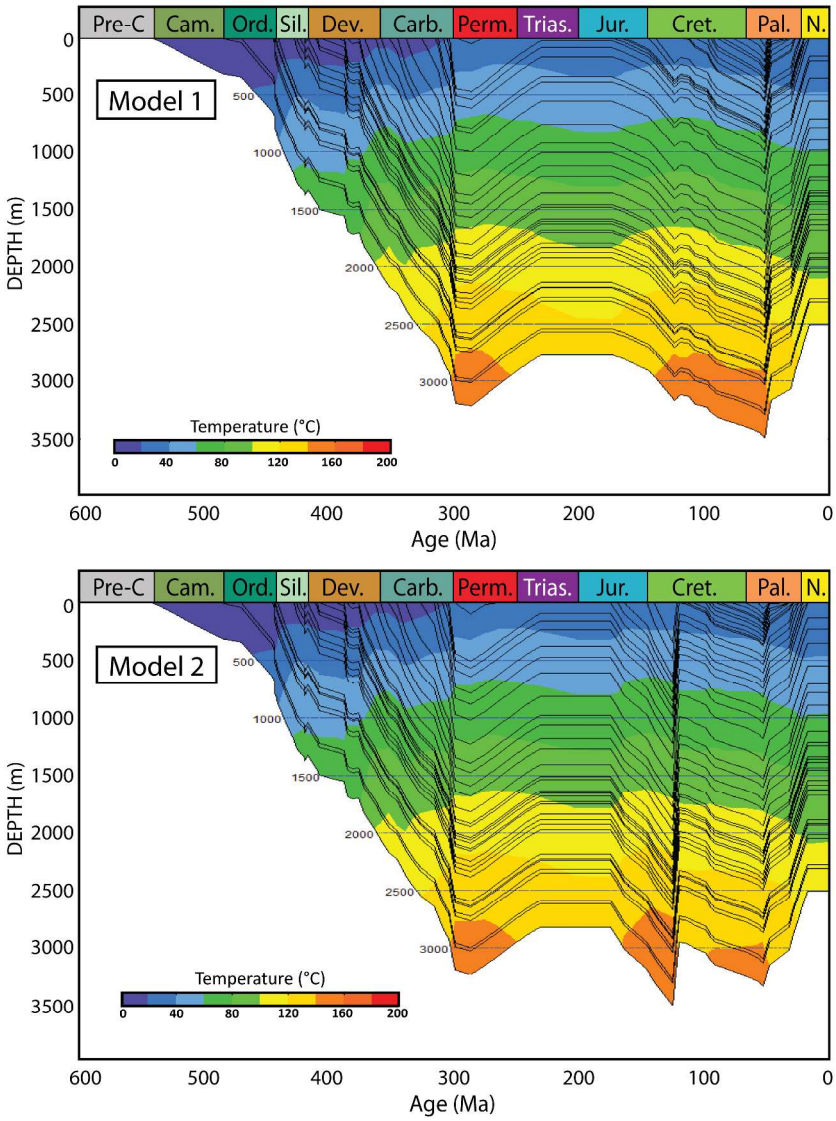

Figure 4: 1D thermal history models for Well A calibrated to thermal maturity and fission-track data. (A) Model 1 assumes maximum burial during the Eocene. (B) Model 2 assumes maximum burial during the Middle Cretaceous at the Austrian tectonic event. Additionally, slightly more Carboniferous deposition in Model 2 (50m) with 25m less Hercynian erosion was required to best match maturity. While these solutions are non-unique, the new data require significant additional burial to match the peak paleotemperature constraints, followed by the onset of significant exhumation during the Eocene. Thermal history modelling was carried out using Genesis.

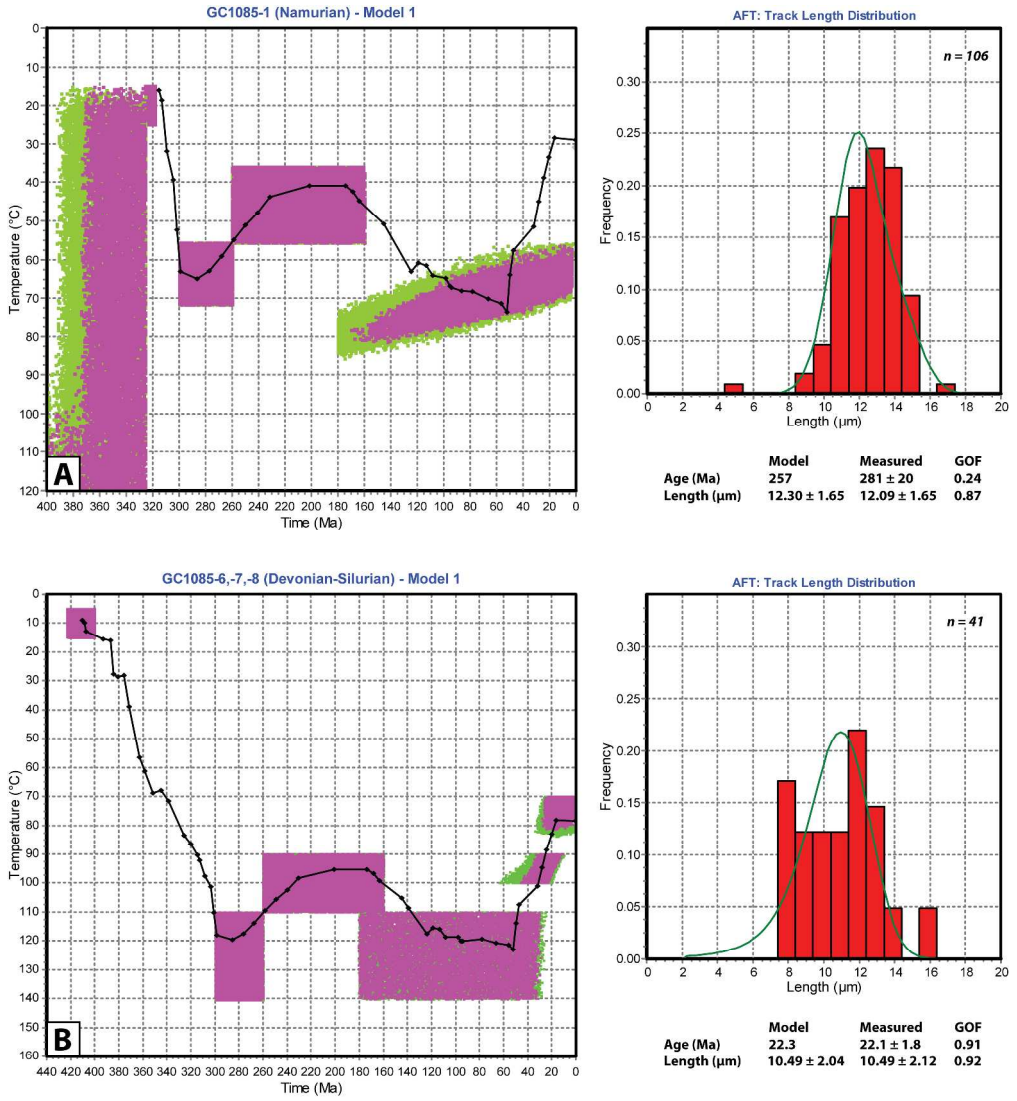

Figure 5

Figure 5: Temperature-time (T-t) histories from Model 1 for (A) the Namurian sample (GC1085-1) and (B) the combined Devonian-Silurian samples (GC1085-6, GC1085-7 and GC1085-8) exported from Genesis into HeFTy. Forward modelling of the T-t pathways in HeFTy provide a very good fit (GOF > 0.85) for the track length distribution in both samples and for the fission-track age in the Devonian-Silurian samples. The goodness-of-fit is lower for the fission-track age in the Namurian sample and this may be due to preservation of pre-depositional inheritance as this sample was not fully annealed during burial.

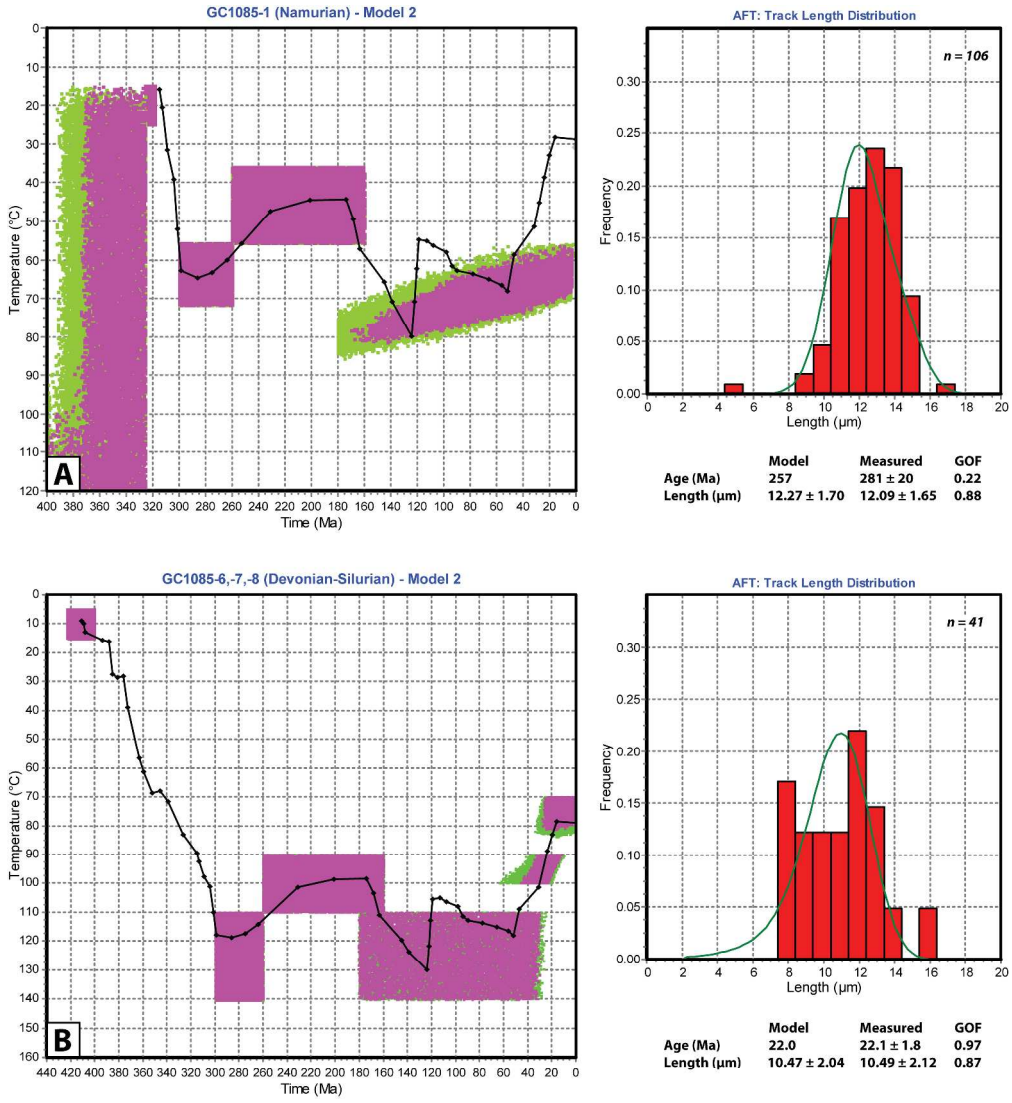

Figure 6

Figure 6: Temperature-time (T-t) histories from Model 2 for (A) theNamurian sample (GC1085-1) and (B) the combined Devonian-Silurian samples (GC1085-6, GC1085-7 and GC1085-8) exported from Genesis into HeFTy. Forward modelling of the T-t pathways in HeFTy provide a very good fit (GOF > 0.85) for the track length distribution in both samples and for the fission-track age in the Devonian-Silurian samples. The goodness-of-fit is lower for the fission-track age in the Namurian sample and this may be due to preservation of pre-depositional inheritance as this sample was not fully annealed during burial.

Figure 7

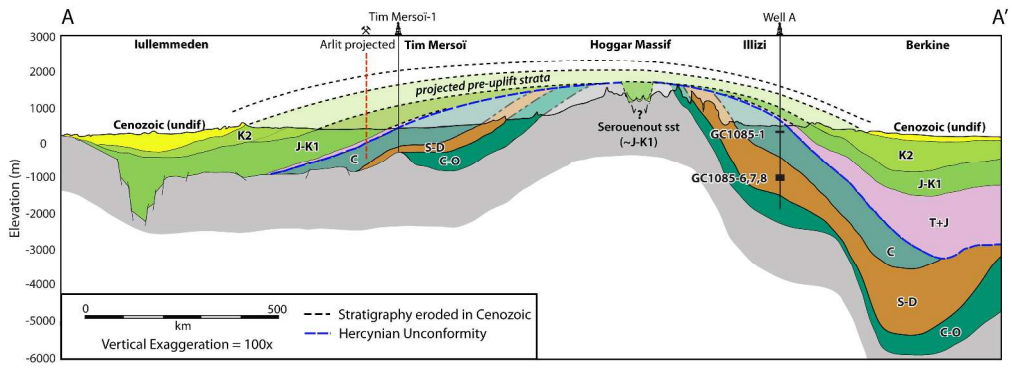

Figure 7: Schematic structural section across the Hoggar Massif from the Berkine Basin in the north to the Iullemmeden Basin in the south (see transect in Fig. 1). Note that the Hoggar had an earlier history of uplift with significant erosion of the Paleozoic sequence during the Hercynian orogeny. Preserved thicknesses are taken from well data (Illizi-Berkine), geology maps and published cross sections (Iullemmeden Basin, Zanguina et al., 1998; Genik, 1993; Dautria & Lesquer, 1989). The eroded stratigraphy of the Tim Mersoï, Hoggar and Illizi regions is projected above the present day surface and calibrated to ~ 1 km of exhumation in Well A, ~ 0.9-1.6 km exhumation in the Serouenout area, and peak burial depths of ~ 1.7-2.3 km for the Visean projected from the Arlit area. Note that the actual magnitude of exhumation in Arlit/Arouta (on the flank of Aïr; Fig. 1) is higher than where it is projected on this section (Carboniferous at surface). Regional data suggests portions of the Central Hoggar may have been inundated with > 1 km of Upper Cretaceous – lower Paleogene sediment. Cenozoic rock uplift across the Hoggar occurred over a distance of >1,500 km from north to south, as indicated by the tilted Cenozoic stratigraphy in the Berkine and Iullemmeden basins. The magnitude of rock uplift, as opposed to exhumation, reaches in excess of 2 km within the core of the Hoggar Massif. Deposition of Upper Eocene-Pliocene sediments (the "Continental Terminal") across Saharan Africa (Kilian, 1931) may represent the onset of clastic sedimentation derived from the growing intracratonic swells.

Table 1: Vitrinite reflectance data from Well A, Illizi basin, Algeria

Well	Analyst	Formation	Depth Interval		Ro Indicator	Sample Count	Vitrinite Reflectance	Bitumen or Chitinozoan Reflectance	Std Dev	Vit. Refl. Equiv.	Peak Paleo-temperature (°C)
			From (m)	To (m)			Ro-Random *(*Ro-Max)*				
Well A	EGS	Namurian	195	350	V	8	0.63	-	0.07	-	104
Well A	EGS	Visean C	450	540	V	12	0.62	-	0.07	-	102
Well A	KK	Tournaisian	720	770	V	10	*(0.61*)*	-	0.05	-	101
Well A	EGS	Tournaisian	800	885	V	9	0.62	-	0.04	-	102
Well A	EGS	Devonian F2	990	1105	V	10	0.67	-	0.05	-	110
Well A	EGS	Devonian MPR	1110	1205	V	7	0.69	-	0.03	-	113
Well A	EGS	Devonian F3	1235	1330	V	14	0.72	-	0.07	-	117
Well A	KK	Devonian F4	1330	1350	V	13	*(0.67*)*	-	0.05	-	110
Well A	EGS	Upper Silurian	1665	1800	B	8	-	0.78	0.05	0.97	142
Well A	EGS	Lower Silurian	1800	1900	B	9	-	0.84	0.07	1.03	146

NOTE: Reflectance data from Well A cuttings was measured by two different contractors (KK = Keiraville Konsultants and EGS = Egs-ploration). No sample count exceeds 14 measurements due to limited sample volume, so maturity estimates must be treated with some caution. Only samples with > 5 measurements are provided here. Measured indicators V= vitrinite; B = bitumen. Measured bitumen reflectance was converted to Ro% equivalent using equation from Schoenherr *et al.* (2007): [$R_{vit} = (R_{bit} + 0.2433) / 1.0495$]. Vitrinite reflectance (and equivalents) were converted to an estimate of peak paleo-temperature assuming a heating rate of 1 °C/Myr (Sweeney & Burnham, 1990).

Table 2: Rock-Eval pyrolysis data from Well A, Illizi basin, Algeria

Well	Formation	Depth (m)		TOC	S_1	S_2	S_3	T_{max}	HI	OI	GP	PI	Calc. Ro% eqv.
		From	To	(wt.%)	mg_{HC}/g_{rock}	mg_{HC}/g_{rock}	mg_{HC}/g_{rock}	°C	mg_{HC}/g_{TOC}	mg_{CO2}/g_{TOC}	mg_{HC}/g_{rock}		
Well A	Devonian F2 Shale	990	1105	1.67	0.39	3.92	0.64	438	235	38	4.31	0.09	0.72
Well A	Devonian MPR	1110	1205	1.69	0.65	4.52	0.57	439	267	34	5.17	0.13	0.74
Well A	Devonian F3	1235	1330	1.26	0.5	3.29	0.46	445	261	37	3.79	0.13	0.85

NOTE: T_{max} to Ro% conversion from Jarvie *et al.* (2001) and Peters *et al.* (2005): [$Ro\%\ eqv=(0.018*T_{max}) - 7.16$]. Rock-Eval data were screened according to criteria of English *et al.* (2015) and Peters & Cassa (1994). TOC: total organic carbon; HI: hydrogen index; OI: oxygen index; GP: genetic potential; PI: production index

Table 3: Apatite fission-track data from Well A, Illizi Basin, Algeria

Sample number	Formation	Stratigraphic Age (Ma)	Depth (m)	Present Day Temp. (°C)	No. of grains	Spontaneous		Induced		P(χ^2)	Dosimeter		F.T. Age (Ma ± 1σ)	Mean Track Length (μm)	Std. dev.	No. of tracks
						ρ_s	N_s	ρ_i	N_i		ρ_D	N_D				
GC1085-1	Namurian	326 - 315	160-200	29	21	1.080	477	1.071	473	11.7%	1.449	2283	281 ± 20	12.09 ± 0.16	1.65	106
GC1085-2	Visean B	347 - 331	600-630	46	6	1.104	98	2.919	259	6.3%	1.450	2283	107 ± 13	10.48 ± 0.68	1.51	5
GC1085-6	Devonian F6C3	406 - 400	1385-1425	76	10	0.370	64	3.646	631	88.5%	1.452	2283	28.9 ± 3.9	10.57 ± 1.45	3.25	5
GC1085-7	Devonian F6C1	417 - 410	1445-1500	79	8	0.274	55	3.069	616	4.4%	1.452	2283	25.4 ± 3.6*	9.79 ± 0.51	1.60	10
GC1085-8	Silurian F6A	423 - 418	1535-1560	82	19	0.180	73	3.030	645	16.1%	1.453	2283	16.9 ± 2.1	10.75 ± 0.41	2.08	26
GC1085-9	Silurian F6M1	426 - 423	1620-1660	85	11	0.464	61	6.478	852	5.6%	1.454	2283	20.4 ± 2.8	11.06 ± 0.41	1.89	21
GC1085-10	Ordovician Unit IV	444 - 439	1915-2117	99	18	0.109	35	3.234	1038	4.4%	1.455	2283	9.6 ± 1.7*	12.59 ± 0.60	2.09	12
GC1085-6, -7, -8 Combined		*423 - 400*	*1385-1560*	*79*	*37*	*0.246*	*192*	*3.177*	*2477*	*5.2%*	*1.452*	*2283*	*22.1 ± 1.8*	*10.49 ± 0.33*	*2.12*	*41*

NOTE: ρ_s - spontaneous track density ($\times 10^6$ cm^{-2}) measured in internal mineral surfaces; ρ_i and ρ_D - induced and dosimeter track density ($\times 10^6$ cm^{-2}) on external mica detectors; N_s, N_i and N_D - number of spontaneous, induced tracks and total number of tracks; P(χ^2) - probability of obtaining $\chi 2$ value for degrees of freedom (where ν = number of crystals – 1). The presented fission-track ages are pooled ages commonly used when P($\chi 2$) > 5% (Galbraith & Laslett, 1993). The two samples with P($\chi 2$) < 5% have central ages of 29.7±5.9 Ma (*GC1085-7*) and 8.5±2.4 Ma (*GC1085-10*).